AGH
IFTJ

CONSIDERATIONS ON THE MÖSSBAUER LINE-WIDTH IN SCATTERING EXPERIMENTS

KRZYSZTOF RUEBENBAUER
WOJCIECH ŻUREK

INSTITUTE OF NUCLEAR PHYSICS AND TECHNIQUES

UNIVERSITY OF MINING AND METALLURGY

CONSIDERATIONS ON THE MOSSBAUER LINE-WIDTH

IN SCATTERING EXPERIMENTS

ROZWAŻANIA NAD SZEROKOŚCIA LINII MOSSBAUEROWSKIEJ

W EKSPERYMENTACH ROZPROSZENIOWYCH

ПОЛУШИРИНА МЭССБАУЕРОВСКОЙ ЛИНИИ В ЭКСПЕРИМЕНТАХ

С РАССЕЯНИЕМ ГАММА ЛУЧЕЙ

Krsysztof Ruebenbauer

Institute of Physics, Jagiellonian University

Wojcieoh Żurek

Institute of Nuclear Physics and Techniques

University of Mining and Metallurgy

Streszczenie

W pracy przedstawiono analizę kształtu linii mössbauerow-
skiej po rozproszeniu w rezonansowej, izotropowej tarczy.
Zostało pokazane, że półszerokość zależy od geometrii rozpra-
szania i że w specjalnych warunkach może być mniejsza od na-
turalnej półszerokości. Półszerokość może być w tych specjal-
nych warunkach zredukowana aż do 0,643 naturalnej półszerokoś-
ci po pojedyńczym rozproszeniu.

Summary

The paper contains an analysis of the Mössbauer line
shape after scattering by a resonance, isotropic target. It
is shown that line-width depends on the scattering geometry
and under special circumstances may be smaller than natural
line-width. Linewidth may be reduced under these special
conditions up to 0.643 natural line-width in a single scatte-
ring process. $\left(author \right)$

3

Резюме

В статье произведено анализ ширины мэссбауеровской линии гамма лучей по рассеянию на резонансовой, однородной фольм. Показано, что полуширина этой линии зависить от геометрии рассеяния и в специальных условах можеть быть меньша чем натуральная полуширина. В этих условях полуширина можеть получить величину 0.643 натуральной полуширины по однократном рассеянию.

Introduction

Scattering geometry is rather less commonly used than the transmission one in Mössbauer experiments, but even on this topic there exists quite abundant literature. On the other hand, only a few experiments were performed to check scattered line shape and these were mainly concerned with hyperfine structure and coherent phenomena. Coherent processes in resonance scattering were treated by many authors, but perhaps in the greatest detail by Hannon and Trammel [8].

In this paper we make an analysis of the scattered line shape assuming that source, target, and absorber are unsplit, homogeneous, and isotropic and that it is possible to neglect coherent processes. We assume isotropy also in the microscopic environment of the Mössbauer nucleus (e.g. no evidence of Goldanski-Karyagin effect).

We assumed also, for simplicity, that source, scatterer, and absorber host lattices are the same.

In this manner the results of the theory presented below reproduce results of the theories treating thick absorbers for the transmissive part of spectrum.
The most detailed analyses for the Mössbauer transmission spectrum were made by Margulies, Ehrman [5] and Ruby, Hicks [7]. We treat the scatterer outgoing beam in good collimation approximation (also the incoming beam), which is of importance in high resolution spectroscopy [6].

The most interesting prediction of the presented theory
is the fact that we may in a fairly simple way obtain a line
narrower than the natural one and without sidebands. This may
be of importance in some kinds of experiment.

Recoilless resonance scattering was investigated by Major
[4] (without considering line-width) and his "negative line-
-widths" results are probably due to great scatterer thickness.
Our $\emptyset$ factor proportional to f^2 (f stands for the Debye-Waller
factor) is in good agreement with Major's [4] results.

The theory presented below may be generally compared (in
its basic ideas) with the work of Andreeva and Kuzmin [9].

1. Theory

1.1. General considerations

The Mössbauer transmission spectrum without hyperfine
splitting, relaxation processes, Goldanski-Karyagin effect,
preferential orientation of crystallities, and interference
processes in the source, target, and absorber may be written
down as follows (neglecting coherent electronic scattering)

$$P_0 (v) = \int_{-\infty}^{\infty} d\omega \; S(\omega) \, e^{-\tau a (\omega - v)} \qquad (1)$$

for well collimated beams. We assume also that source, target,
and absorber are homogeneous and isotropic and that the energy

shift is the same for source, target, and absorber. The source
is thin in the Mössbauer sense and is not moving versus the
target. T is the absorber thickness and a $(\omega - v)$ may be
written as:

$$a(\omega - v) = \frac{\Gamma^2}{4} \frac{1}{(\omega - v)^2 + \Gamma^2/4} , \qquad (2)$$

where Γ is the natural half-width of the excited level (for
simplicity we assume that it is first excited level), ω is
the energy deviation from the transition energy, and v is
the Doppler shift energy between source and absorber.

For line-width considerations we may use a spectrum
normalized to the form:

$$\bar{P}_0 (v) = \frac{P_0 (\infty) - P_0 (v)}{P_0 (\infty) - P_0 (0)} \qquad (3)$$

S (ω) is the density matrix of the incoming beam in the
energy representation. This matrix is diagonal because
Mössbauer scattering is an energy conserving process. S (ω)
has such a property that S $(\omega) \neq$ S $(-\omega)$.

Let us consider scattering of the well-collimated beam
Z (ω) from the slab in the geometry illustrated by Fig. 1.
The x, y, dimensions of the slab we assume to be infinite.
We take into consideration only this part of scattered photons
which are moving along the z axis. We also neglect all con-
siderations connected with the luminosity of necessary

7

collimators (for simplicity we assume that this luminosity is equal to 1). Under these conditions we may write down $Z(\omega)$ as:

$$Z(\omega) = (f_s \sin\beta_0)\, \frac{\Gamma}{2\pi} \frac{1}{\omega^2 + \Gamma^2/4}\ , \qquad (4)$$

where f_s is the source Debye-Waller factor. We use such a normalization that the number of photons at any energy (resonant and non-resonant) coming per unit time and unit area of the surface perpendicular to the $Z(\omega)$ is equal 1.

The transmitted beam may be now described by the relation (Figs 1, 2):

$$T(\omega) = \delta(\tfrac{\pi}{2} - \beta_0)\, \delta(\varphi)\, Z(\omega)\, e^{-\alpha(\omega)\varrho d/\sin\beta_0}, \qquad (5)$$

where ϱ is target density and:

$$\alpha(\omega) = t_0 \delta(\omega) + \mu\ , \qquad (6)$$

where μ stands for the target electronic absorption coefficient for Mössbauer photons and may be expressed as:

$$\mu = \frac{N}{A}\,\delta_e\ , \qquad (7)$$

where N is the Avogadro number, A is the weighted average of mass numbers of elements building the target, and δ_e is the weighted average of electronic absorption cross-sections

of elements in the target.

$$t_o = \frac{N}{A} \, pf \, \mathcal{6}_o, \qquad (8)$$

where p is the molecular abundance of Mössbauer isotope, f is the Debye-Waller factor of the target, and $\mathcal{6}_o$ is the resonance cross-section (including spins, energy, and total internal conversion dependence).

Now $\mathcal{6}(\omega)$ may be expressed as:

$$\mathcal{6}(\omega) = \frac{\Gamma^2}{4} \frac{1}{\omega^2 + \Gamma^2/4} \qquad . \qquad (9)$$

Probability of scattering of the photon with energy per unit length of its path in the target may be described by the function:

$$g(\omega) = \emptyset \, \mathcal{6}(\omega), \qquad (10)$$

where

$$\emptyset = \mathcal{S} \frac{N}{A} \, p \, f^2 \, \mathcal{6}_o \frac{1}{1 + \alpha_{tot}} \qquad . \qquad (11)$$

α_{tot} is the total internal conversion coefficient.
The expression for $\emptyset$ is derived from the natural assumption that after absorption we are interested only in reemission of the recoilless photon. (We do not consider background problems).

9

We also define two very useful expressions:

$$F(\omega, s) = e^{-\alpha(\omega)[d-s]\varsigma} \qquad . \qquad (12)$$

and

$$G(\omega, s) = Z(\omega)\, g(\omega)\, e^{-\alpha(\omega)\varsigma\, s/\sin\beta_0} \qquad , \qquad (13)$$

where $0 \leqslant s \leqslant d$.

$F(\omega, s)$ describes the transmission of photons scattered at the layer s (Figs 2,3) and moving along the s axis.
$G(\omega, s)$ describes the energy profile of primary photons scattered at the layer s (Fig. 2) in the position of this layer.

It seems natural to expand $S(\omega)$ as follows:

$$S(\omega) = \sum_{j=1}^{\infty} S_j(\omega), \qquad (14)$$

where j is the index of the scattering multiplicity.

$$S_1(\omega) = \int_0^d ds\, G(\omega, s)\, F(\omega, s) \qquad (15)$$

$$= Z(\omega) e^{-\alpha(\omega)\varsigma d} \frac{g(\omega)\,\sin\beta_0}{\alpha(\omega)\,[1-\sin\beta_0]} \times$$

$$\left[1 - e^{-\alpha(\omega)\varsigma d\,(\frac{1-\sin\beta_0}{\sin\beta_0})}\right]$$

and for $j>1$ we may write down (Fig. 3):

$$S_j(\omega) = \int_0^d ds_1 \ldots ds_j \; G(\omega, s_1) \prod_{l=1}^{j-1} K(\omega, z, s_l, z_{l+1}) \times$$

$$P(\omega, s_j). \tag{16}$$

$K(\omega, s_l, s_{l+1})$ describes the probability that the photon with energy ω just scattered at the layer s_l will be next scattered at the layer s_{l+1}.
$K(\omega, s_l, s_{l+1}) = K(\omega, s_{l+1}, s_l)$, of course.

1.2. Calculation of the function $K(\omega, s_0, s)$

Fig. 4 shows how radiation propagates from any point P of plane s_0 to the elementary volume dV lying in the plane s. Volume dV may be expressed in spherival coordinates as follows (Fig. 4):

$$dV = r^2 \sin \theta \, dr \, d\theta \, d\varphi. \tag{17}$$

Integrating over φ makes:

$$dV' = \int_0^{2\pi} r^2 \sin \theta \, dr \, d\theta \, d\varphi = 2\pi r^2 \sin \theta \, dr \, d\theta. \tag{18}$$

dV' may be rewritten as (Figs 4, 5):

$$dV' = 2\pi (s - s_0)^2 \frac{\sin \theta}{\cos^3 \theta} \, ds d\theta, \tag{19}$$

where we are using relations:

11

$$r = (z - z_0)/\cos \theta \tag{20}$$

and

$$dr = dz/\cos \theta. \tag{21}$$

Radiation intensity with the distance r from the scattering point is attenuated by the factor:

$$J(r,\omega) = \frac{1}{4\pi r^2} e^{-\alpha(\omega)\varsigma r} \tag{22}$$

The last expression may be rewritten as:

$$J(/z-z_0/,\omega) = \frac{\cos^2 \theta}{4\pi (z-z_0)^2} e^{-\alpha(\omega)\varsigma /z-z_0//\cos \theta} \tag{23}$$

Now we may write down the probability that the photon scattered at P (in the plane z_0) will be next scattered in the plane z and that this photon is coming to z from z_0 at the angle θ and any angle φ. This may be written down as:

$$k(\omega, z_0, z, \theta) \, dz \, d\theta = J(/z-z_0/,\omega) \, g(\omega) \, dV'$$

$$= \frac{1}{2} g(\omega) \, t_g(\theta) e^{-\alpha(\omega)\varsigma /z-z_0//\cos \theta} \, dz \, d\theta \tag{24}$$

θ range is shown in Fig. 6. Hence, we have:

$$K(\omega, z_0, z) = \int_0^{\pi/2} k(\omega, z_0, z, \theta) \, d\theta \tag{25}$$

$$= \frac{1}{2} g(\omega) \int_{0}^{\pi/2} d\theta \, tg(\theta) e^{-\alpha(\omega) g /z-z_0// \cos \theta}$$

Let us define:

$$A = \alpha(\omega) g /z-z_0/ \; > \; 0. \tag{26}$$

Function $tg(\theta)e^{-A/\cos \theta}$ may be rewritten as:

$$tg(\theta)e^{-A/\cos \theta} = \frac{\sin \theta}{\cos \theta \, e^{A/\cos \theta}} = \frac{L(\theta)}{M(\theta)} \tag{27}$$

Hence, we have $(\theta \in [0, \frac{\pi}{2}])$:

$$\lim_{\theta \to 0} \frac{L(\theta)}{M(\theta)} = 0, \tag{28}$$

$$\lim_{\theta \to \frac{\pi}{2}} L(\theta) = 1 \text{ and} \tag{29}$$

$$M(\theta) = \cos \theta + A + \sum_{l=2}^{\infty} \frac{A^{l}}{l!} \frac{1}{\cos^{(l-1)}\theta} \tag{30}$$

$$\lim_{\theta \to \frac{\pi}{2}} M(\theta) = A + \lim_{\theta \to \frac{\pi}{2}} \sum_{l=2} \frac{A^{l}}{l} \frac{1}{\cos^{(l-1)}\theta} = \infty. \tag{31}$$

Thus, it is shown that:

$$\lim_{\theta \to \frac{\pi}{2}} \frac{L(\theta)}{M(\theta)} = 0 \quad . \tag{32}$$

Under these conditions we may expand $tg\,(\theta)$ and write down relation:

$$\int_0^{\pi/2} d\theta\, tg\,(\theta) e^{-A/\cos\theta} = \sum_{n=1}^{\infty} \frac{2^{2n}(2^{2n}-1)B_n}{(2n)!} \lim_{\substack{\varepsilon \to 0 \\ \varepsilon > 0}} \int_0^{\pi/2-\varepsilon} d\theta\, x$$

$$\theta^{2n-1} e^{-A/\cos\theta}, \tag{33}$$

where B_n are Bernoulli's numbers expressed by the formula:

$$B_n = \frac{2(2n)!}{\pi^{2n}(2^{2n}-1)} \sum_{k=1}^{\infty} 1/(2k-1)^{2n} \tag{34}$$

From (33) and (34) we have:

$$\int_0^{\pi/2} d\theta\, tg\,(\theta) e^{-A/\cos\theta} = 2\sum_{n=1}^{\infty} \left(\frac{2}{\pi}\right)^{2n} R_n \lim_{\substack{\varepsilon \to 0 \\ \varepsilon > 0}} \int_0^{\pi/2-\varepsilon} d\theta\, \theta^{2n-1} x$$

$$e^{-A/\cos\theta}, \tag{35}$$

where:

$$R_n = \sum_{k=1}^{\infty} 1/(2k-1)^{2n} \tag{36}$$

14

Finally, we may write down:

$$K(\omega, z_0, z) = g(\omega) \sum_{n=1}^{\infty} (\tfrac{2}{3})^{2n} R_n \lim_{\substack{\varepsilon \to 0 \\ \varepsilon > 0}} \int_0^{\pi/2 - \varepsilon} d\theta\, \theta^{2n-1} \quad x$$

$$e^{-\alpha(\omega)\rho |z-z_0| / \cos\theta} \tag{37}$$

Integration over θ may now be made using any efficient numerical method (e.g. the Gauss-Legendre method).

It is true, of course, that:

$$\lim_{\theta \to 0} \theta^{2n-1} e^{-A/\cos\theta} = 0 \tag{38}$$

and

$$\lim_{\theta \to \frac{\pi}{2}} \theta^{2n-1} e^{-A/\cos\theta} = 0 \tag{39}$$

1.3. Some properties of the function $S_1(\omega)$

It is clear, of course, that:

$$\lim_{\beta_0 \to 0} Z(\omega) = 0 \tag{40}$$

and

$$\lim_{\beta_0 \to \frac{1}{2}} Z(\omega) = f_s \frac{\Gamma}{2\pi} \cdot \frac{1}{\omega^2 + \Gamma^2/4} \quad . \tag{41}$$

So:

$$\lim_{\beta_0 \to 0} S_1(\omega) = 0 \quad . \tag{42}$$

On the other hand, we may write down:

$$\lim_{\beta_0 \to \frac{\pi}{2}} S_1(\omega) = Z(\omega) \, g(\omega) \, d \, e^{-\alpha(\omega)\beta d} \tag{43}$$

$$= f_s \frac{\Gamma}{2\pi} \cdot \frac{g(\omega) \, d \, e^{-\alpha(\omega)\beta d}}{\omega^2 + \Gamma^2/4}$$

Comparing (37), (16), and (10) it is easy to show that:

$$\lim_{\emptyset \to 0} S(\omega) = S_1(\omega), \tag{44}$$

but equation (44) will also be satisfied under a slightly weaker restriction $\emptyset \, d \to 0$ (Fig. 1).

So, we.may rewrite (44) as:

$$\lim_{\emptyset \, d \to 0} S(\omega) = S_1(\omega) \quad . \tag{45}$$

Remembering these conditions, we may write down:

$$\lim S_1 (\omega) = Z (\omega) q(\omega) \rho d \qquad (46)$$

$$\beta_0 \to \frac{\pi}{2} \, , \, d \to 0$$

$$= (\frac{f_s \Gamma^3 \not{p} d}{8 \pi}) \cdot \frac{1}{(\omega^2 + \Gamma^2/4)^2} \quad .$$

Function $\dfrac{\Gamma^2}{4} \dfrac{1}{\omega^2 + \Gamma^2/4}$ has half-width Γ and this is

the natural half-width of the Mössbauer source line.
Function (46) is proportional to the value

$$(\Gamma^4/16) \Big/ (\omega^2 + \Gamma^2/4)^2 \quad .$$

The half-width Δ of this latter function may be derived
from the expression:

$$\frac{\Gamma^4}{16} \quad \frac{1}{(\frac{\Delta^2}{4} + \frac{\Gamma^2}{4})^2} = \frac{1}{2} \quad . \qquad (47)$$

Hence we have:

$$\Delta^4 + 2 \Delta^2 \Gamma^2 - \Gamma^4 = 0 \qquad (48)$$

and for a physical meaningful solution we obtain

$$\Delta = \Gamma (\sqrt{2} - 1)^{\frac{1}{2}} \qquad (49)$$

$$= \Gamma \cdot 0.643.$$

Thus it is clearly shown that for $\beta_0 \to \frac{\pi}{2}$ and $d \to 0$ the scattered line is 35.7% narrower than the natural line (see also [9]).

This is consistent with consideration of the time correlation function for the nuclear Hamiltonian of the Mössbauer level. For a single nucleus such a function is proportional to e^{-pt}, where $p = \Gamma/2 + i\omega_0$, where ω_0 is transition energy. The energy profile for such a function is proportional to its real part of the Fourier transform and may be written as something proportional to $1/[(\Gamma/2)^2 + \Omega^2]$, where $\Omega = \omega - \omega_0$. The correlation function for a state consisting of two nuclear levels has a form proportional to $\int_0^t e^{-p\tau} e^{p(t-\tau)} d\tau$ and its energy profile is, of course, proportional to $1/[(\Gamma/2)^2 + \Omega^2]^2$.

We may also consider multiple scattering (with multiplicity m) under the conditions mentioned above for all $m = 1, 2 \ldots m'$. These conditions may be arranged repeating m' times the situation shown in Fig. 1. Hence, we have:

$$\lim S^{(m')}(\omega) = (\frac{f_a \Gamma}{2\pi}) \prod_{m=1}^{m'} \phi_m d_m \frac{(\Gamma^2/4)^{m'}}{(\omega^2 + \Gamma^2/4)^{(m'+1)}} . \quad (50)$$

$$\left. \begin{array}{c} \beta_{om} \to \frac{\pi}{2} \\[2mm] \phi_m d_m \to 0 \end{array} \right\} \quad m = 1, 2, \ldots m'$$

We now obtain for half-width the following expression

$$\frac{(\Gamma^2/4)^{m'}}{\left[(\Delta_{m'}/2)^2 + \Gamma^2/4\right]^{(m+1)}} = 2/\Gamma^2 \qquad (51)$$

and

$$2 = \left(\frac{\Delta^2_{m'}}{\Gamma^2} + 1\right)^{(m'+1)} \qquad (52)$$

From (52) we see at once that for $m' \to \infty$ $\Delta_{m'}$ converges to 0. This is connected, of course, with enormous loss of intensity.

The multiple scattering described above is also consistent with the time correlation function picture. Such a function for m' multiplicity may be written as something proportional to

$$\int_0^t d\tau_{m'} e^{-p(t-\tau_{m'})} \int_0^{\tau_{m'}} d\tau_{m'-1} e^{-p(\tau_{m'} - \tau_{m'-1})} \cdots$$

$$\int_0^{\tau_2} d\tau_1 e^{-p(\tau_2 - \tau_1)} e^{p\tau_1}$$

and the real part of its Fourier transform has a form proportional to $1/(\Omega^2 + \Gamma^2/4)^{(m'+1)}$.

2. Discussion of some experimental possibilities·

It seems clear that for preliminary experiments should be selected the 14.41 keV line in ^{57}Fe (^{57}Co) which has practically M 1 transition (so we may forget about interference between Mössbauer and photoelectric absorption amplitude). From various single line sources and absorbers material should be selected with a high enough Debye-Waller factor and with a small spread of isomer shifts. Thus, for source, target, and absorber the same type of material must be used. For metallurgical properties, it seems that the best one may be the Pd-Fe system. As an example we calculated $S_1(\omega)/S_1(0)$ versus ω/Γ and $\bar{P}_{01}(v)$ versus v/Γ for several β_v (Fig. 7) and also $\varkappa_1$, $\Delta S_1/\Gamma$ and $\Delta \bar{P}_{01}/\Gamma$ versus β_0 (Fig. 8), where ΔS_1 is the half-width of the scattered $S_1(\omega)$ line, $\Delta \bar{P}_{01}$ is the half-width of the spectrum $\bar{P}_{01}(v)$, and $\varkappa_1$ is defined as:

$$\varkappa_1 = \int_{-\infty}^{\infty} d\omega\, S_1(\omega) = 2 \int_{0}^{\infty} d\omega\, S_1(\omega) \tag{53}$$

Generally:

$$\varkappa = \int_{-\infty}^{\infty} d\omega\, S(\omega) = 2 \int_{0}^{\infty} d\omega\, S(\omega) \tag{54}$$

Thus, $\varkappa$ describes the scattering efficiency.
Numerical values were adopted from literature for a ^{57}Co (Pd) source and $Fe_{0.05}\,Pd_{0.95}$ (at.%) alloy target and absorber.

We assumed that this alloy is enriched up to 95 (at. %) in ^{57}Fe. We assumed also that source, target, and absorber are kept in the same temperature very close to 293 K. All adopted values are listed in Table I.

Table I

Values adopted for calculating curves shown in Figs 7 and 8.

Parameter	Units	Value	Ref. and Remarks
N	mole^{-1}	6.0249×10^{23}	
A	g/mole	$103 \cdot 93$	Weighted average
$f_s = f$	—	0.652	[1]
T	—	1.0	
p	—	0.0475	
$\rho \approx \rho_{Pd}$	g/cm^3	12.0	
σ_o	cm^2	2.569×10^{-18}	[2]
σ_e	cm^2	6.646×10^{-21}	Weighted averaged and interpolated [3]
d_{tot}	—	8.18	[2]
β	cm^{-1}	32.750	
μ	cm^2/g	38.527	
t_o	cm^2/g	461.2	
d	cm	9.03×10^{-5}	$t_o \rho d = 0.5;$ $\beta d = 2.959 \times 10^{-3}$

Acknowledgments

References

[1] J.Bara "Remarks on the Application of the Mössbauer
Effect in the Investigations of Crystal Microdynamics"
Tihany (1969).

[2] J.G.Stevens, V.E.Stevens "Mössbauer Effect Data Index -
1970" London (1971).

[3] C.M.Davisson "Gamma-Ray Attenuation Coefficients" in
K.Siegbahn (editor) "Alpha, Beta and Gamma-Ray Spectros-
copy" Vol. 1. p.827. Amsterdam (1966).

[4] J.K.Major "Recoil-free Resonant and Non-resonant Scatte-
ring from ^{57}Fe" Nucl. Phys. $\underline{33}$ (1962) 323.

[5] S.Margulies, J.R.Ehrman "Transmission and Line Broadening
of Resonance Radiation Incident on a Resonance Absorber"
Nucl. Instr. Meth. $\underline{12}$ (1961) 131.

[6] N.N.Delyagin, K.P.Mitrofanow and V.J.Nesterov "On the
Real Shape of Spectral Lines in Mössbauer Spectroscopy"
Nucl. Instr. Meth. $\underline{100}$ (1972) 315.

[7] S.L.Ruby, J.M.Hicks "Line Shape in Mössbauer Spectro-
     scopy" Rev. Sci. Instr. 33 (1962) 27.

[8] J.P.Hannon, G.T.Trammell "Mössbauer Diffraction. II.Dyna-
     mical Theory of Mössbauer Optics" Phys. Rev. 186 (1969)
     306.

[9] M.A.Andreeva, R.N.Kuzmin "Narrowing of the Mössbauer
     Line" Proc. of the Conf. on the Application of the
     Mössbauer Effect – Tihany (1969).
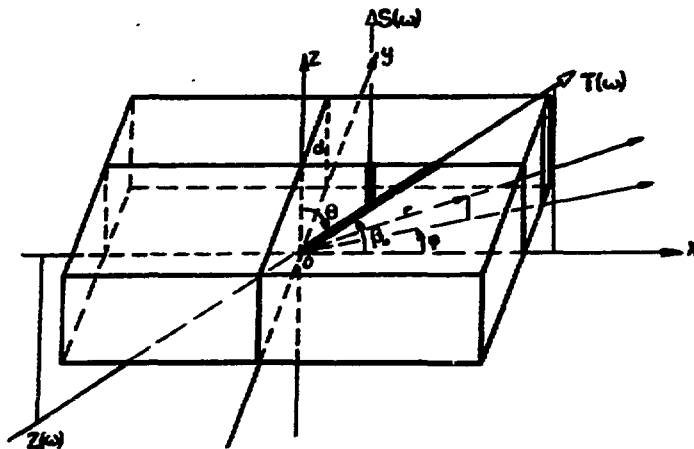
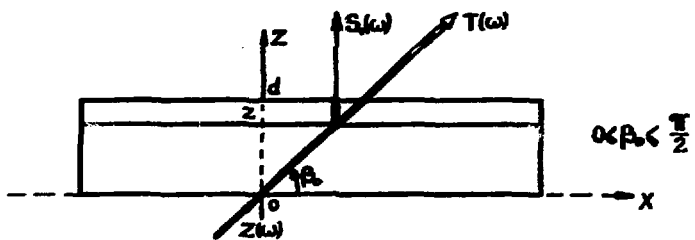Fig. 1. Schematic diagram of the considered
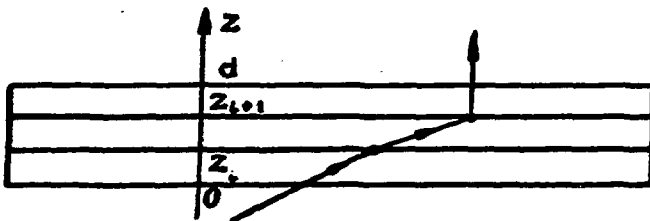scattering geometry.

Fig. 2. Path of the single scattered photon.

Fig. 3. Photon path between two scattering
layers in the target.
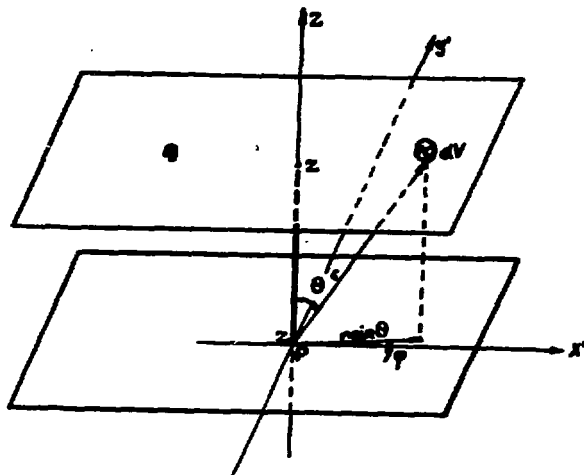
Fig. 4. Diagram showing all possible paths of the
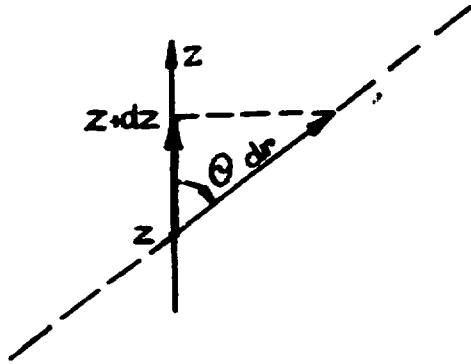photon between two scattering layers.

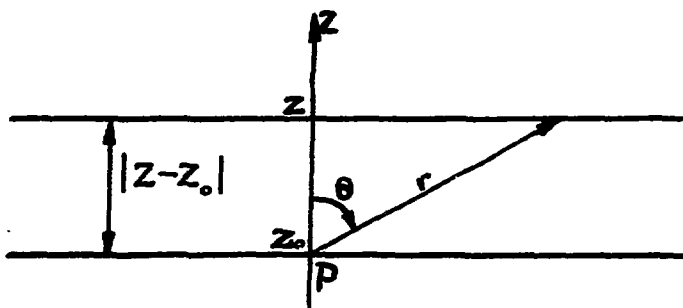Fig. 5. Projection of the photon path direction on the Z axis.

Fig. 6. Diagram showing the range of the θ
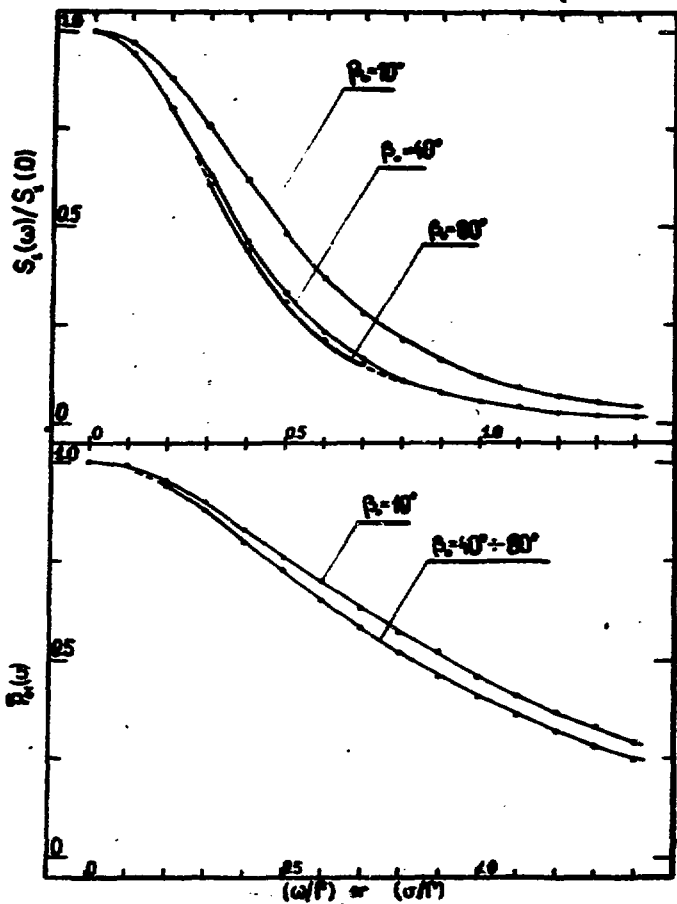angle variation.

29

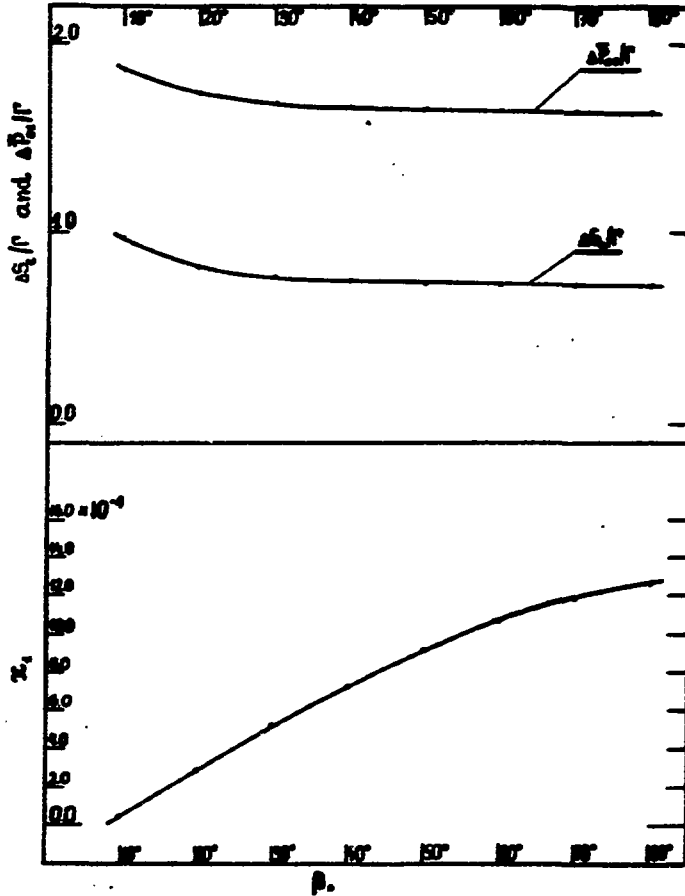Fig. 7. $S_1(\omega)/S_1(0)$ and $P_{o1}(v)$ for several β_o calculated for parameters listed in the Table I.

Fig. 8. $\Delta S_1/\Gamma$, $\Delta \bar{P}_{\rho 1}/\Gamma$ and $\mathcal{K}_1$ calculated for various β_o and parameters listed in Table I.